Emergence of Van Hove singularity and topological states in Pb_3Bi/Ge(111) Rashba systems

Leiqiang Li,[1] Shang Ren,[1,*] Wei Qin,[1,2] Shunhong Zhang,[1] Xiangang Wan,[3] Yu Jia,[4] Ping Cui,[1,5,†] and Zhenyu Zhang[1,†]

[1]*International Center for Quantum Design of Functional Materials (ICQD), Hefei National Laboratory for Physical Sciences at Microscale (HFNL), and CAS Center for Excellence in Quantum Information and Quantum Physics, University of Science and Technology of China, Hefei, Anhui 230026, China*

[2]*Department of Physics, The University of Texas at Austin, Austin, Texas 78712, USA*

[3]*National Laboratory of Solid State Microstructures and School of Physics, Nanjing University, Nanjing 210093, China*

[4]*School of Physics and Engineering, Zhengzhou University, Zhengzhou 450001, China*

[5]*Key Laboratory of Strongly-Coupled Quantum Matter Physics, Chinese Academy of Sciences, School of Physical Sciences, University of Science and Technology of China, Hefei, Anhui 230026, China*

(Received 24 January 2020; revised 4 June 2020; accepted 6 July 2020; published 24 July 2020)

It has been shown recently that the coexistence of Van Hove singularity and geometric phase in Pb_3Bi/Ge(111) as a prototypical Rashba system can result in chiral topological superconductivity [W. Qin, L. Li, and Z. Y. Zhang, Nat. Phys. **15**, 796 (2019)]. Here, we use first-principles calculations to systematically investigate the structural, electronic, and topological properties of the Pb_3Bi/Ge(111) alloyed systems by considering not only the configuration that harbors topological superconductivity considered previously (labeled as the T_1 phase) but also two other energetically nearly degenerate configurations with high symmetries (labeled as H_3 and T_4). We first show that all the three structural configurations have giant Rashba-type spin splittings, resulting from the strong spin-orbit coupling effect of the heavy elements (Pb, Bi) together with inversion symmetry breaking. Next, we demonstrate that each of the saddle- or paraboliclike band dispersions can lead to the emergence of Van Hove singularities, whose positions can be substantially tuned by the giant Rashba effect to the vicinity of the Fermi level. Furthermore, we reveal the existence of topological states in both the H_3 and T_4 phases, and the corresponding Rashba-induced band gaps are given by 25 and 50 meV, respectively. Given the energetic affinity of the three phases, these findings suggest the feasibility of realizing quantum phase transitions between quantum spin Hall effect and topological superconductivity within the same materials platform. The present study is expected to give new insights in searching for topological quantum states including 2D topological superconductivity based on Rashba systems.

DOI: 10.1103/PhysRevB.102.035150

I. INTRODUCTION

Rashba effects are characterized by the momentum-dependent spin splittings of the energy bands of crystalline solids. Such effects are usually more pronounced in systems of reduced dimensionality, such as at the two-dimensional (2D) surfaces of bulk materials or the interfaces of heterostructures [1–4]. Physically, Rashba effects arise from the combination of the inherent spin-orbit coupling (SOC) of the constituent elements and inversion-symmetry breaking of the internal crystal potential at the surfaces or interfaces [5–8]. In the past decades, Rashba effect has attracted extensive research attention due to its distinct roles in spintronics [9]. Earlier studies of Rashba effects were mainly focused on their manifestations in systems containing heavy elements, including their surfaces [2,6], overlayers [8,10,11], and heterostructures [3]. More recently, the Rashba effect has been exploited in studies of much broader physical phenomena, such as topological superconductivity induced by proximity effects [12–17] that may serve as an ideal platform for realizing and manipulating Majorana fermions [18–20].

Among these Rashba systems, one representative class of materials is the thin films of Pb [11,21,22] or $Pb_{1-x}Bi_x$ alloys [23–25]. Since both Pb and Bi atoms possess large atomic SOC, the corresponding thin films or alloyed systems were demonstrated to host huge Rashba SOC splittings when grown on a proper substrate [8,11,22,24,26,27]. Moreover, both the atomic thin films of Pb and $Pb_{1-x}Bi_x$ alloys grown on Si(111) or Ge(111) also possess superconductivity, with the superconducting transition temperature tunable by the Pb film thickness or the Bi concentration [23,28–32]. In the more recent study of Pb_3Bi/Ge(111) [33], we have further demonstrated that the interplay between the Rashba effect and Van Hove singularity (VHS) can give rise to chiral topological superconductivity (TSC). The vital role of VHS for realizing superconductivity has also been proposed in single-layer graphene [34] or realized in twisted bilayer graphene [35]. It is thus highly desirable to carry out more systematic studies of such Rashba systems that also harbor VHS in their band structures and may possess intriguing topological and/or superconducting properties, with the 2D $Pb_{1-x}Bi_x$ alloyed films as the concrete example of the present study.

*Present address: Department of Physics and Astronomy, Rutgers University, Piscataway, New Jersey 08854, USA.

†Corresponding authors:
cuipg@ustc.edu.cn; zhangzy@ustc.edu.cn

In this paper, we use density functional theory (DFT) to investigate the structural, electronic, and topological properties of the Pb_3Bi alloy grown on the Ge(111) substrate. In addition to the T_1 configuration studied before [33], here two extra energetically nearly degenerate configurations are identified and fully investigated, labeled as H_3 and T_4. We first show that there exist giant Rashba-type spin splittings in the band structures of all the three structural configurations, due to the presence of the heavy elements (Pb and Bi) together with the inversion symmetry breaking. Secondly, we reveal that each of the saddlelike and paraboliclike band dispersions can lead to the emergence of VHS, whose positions can be substantially tuned by the giant Rashba effect to be within the vicinity of the Fermi level. Moreover, we identify that the H_3 and T_4 phases harbor topological edge states and can be qualitatively characterized as topologically nontrivial quantum spin Hall phases. Detailed hybrid functional calculations reveal that, for the H_3 and T_4 phases, the Rashba-induced band gaps can be 25 and 50 meV, respectively. We also discuss the feasibility of realizing quantum phase transitions between topological superconductivity and quantum spin Hall effect within the same materials platform. Collectively, these findings may prove to be instrumental in searching for new materials systems that harbor topological quantum states including in particular 2D topological superconductors.

This paper is organized as follows. In Sec. II, we present the computational methods employed. The main DFT results are given in Sec. III, where the physics involved in giant Rashba splittings, the existence of VHS, and the corresponding topological states in the T_1, H_3, and T_4 configurations are elucidated. In Sec. IV, we discuss the feasibility of our Rashba systems in hosting both topological edge states and superconductivity, as well as aspects related to physical realizations of these predictions. Finally, we summarize our results in Sec. V.

II. COMPUTATIONAL METHODS

Our DFT calculations were carried out using the Vienna *ab initio* simulation package (VASP) [36,37], where the projector-augmented-wave (PAW) method [38,39] was adopted, and the generalized gradient approximation (GGA) in the framework of Perdew-Burke-Ernzerhof (PBE) [40] was chosen for the exchange-correlation functional. The van der Waals (vdW) correction with the DFT-D3 method [41] was included in all calculations. The plane-wave cutoff energy was set to 400 eV for all the calculations. We construct a slab model containing four Ge bilayers in the $\sqrt{3}\times\sqrt{3}$ $R30^\circ$ supercells to simulate the Ge(111) surface, with the bottom Ge atoms passivated by H atoms. The optimized lattice constants of bulk Ge are $a = b = c = 4.073$ Å. The lattice constants of a and b are fixed in our subsequent simulations with the Pb-Bi overlayer. A $7\times7\times1$ Monkhorst-Pack k-point mesh was used for the $\sqrt{3}\times\sqrt{3}$ $R30^\circ$ unit cell. The vacuum layers were more than 15 Å to ensure decoupling between neighboring slab images. During the relaxation, the bottom Ge bilayer and hydrogen atoms were fixed to their respective bulk positions (see Fig. 1), while all other atoms were allowed to relax until the corresponding forces were smaller than 0.01 eV/Å. To obtain more reliable electronic band gaps, the HSE06 (Heyd, Scuseria, and Ernzerhof) [42] hybrid functional was used. To investigate the topological properties in the Pb_3Bi/Ge(111) systems, we calculate the Z_2 invariant via the Wannier charge centers [43] and construct the edge Green's function of the semi-infinite lattice model [44] from maximally localized Wannier functions [45] as implemented in the WannierTools package [46].

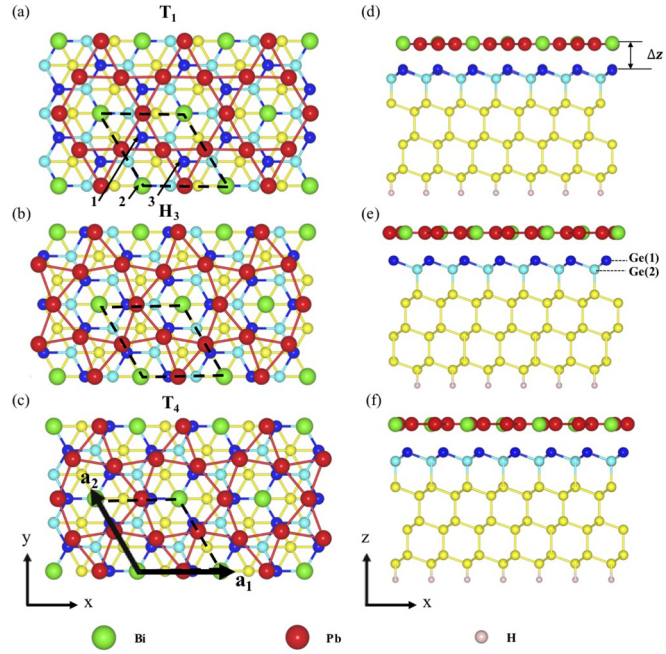

FIG. 1. Top and side views of the Pb_3Bi/Ge(111) systems in the (a), (d) T_1, (b), (e) H_3, and (c), (f) T_4 configurations, where the unit cells are highlighted by the black dashed lines. The numbers 1, 2, 3 in (a) denote the positions of the three Ge atoms in the Ge(1) layer within a unit cell. The primitive lattice vectors $\vec{a}_1$ and $\vec{a}_2$ are shown in (c).

III. RESULTS

A. Atomic configurations and energetics of the Pb_3Bi/Ge(111) systems

Earlier studies demonstrated that the (4/3)-monolayer coverage of Pb atoms on the Si(111) or Ge(111) surface has two energetically competing configurations, known as the H_3 and T_4 structures [47–50]. Recently, superconductivity has been observed in monolayer Pb film grown on Si(111) [30,31]. Yet to date, no evidence suggests that the pure atomic-layer Pb films can achieve topological superconductivity. On the other side, it is well-known that SOC plays a vital role in realizing topologically nontrivial properties. We therefore consider doping the heavier Bi atoms into the monolayer Pb films to investigate the potential nontrivial topology in such superconducting thin films. Here we mainly focus on the substitution of Pb located at the high symmetric position by Bi, labeled as T_1, H_3, and T_4 [see Figs. 1(a)–1(c)]. The nomenclature also follows the Pb/Si(111) case [47–50], namely, the T_1, H_3, and T_4 means that the Bi atom located on the top site, hollow-fcc site, and hollow-hcp site of the Ge (111) substrate, respectively. Justifications of this choice, as well

TABLE I. Atomic distances (d) and vertical spacings (Δz) of the T_1, H_3, and T_4 configurations, both in Å. The labels of the atoms are shown in Fig. 1. Here, a negative value in Δz indicates a lowering of the respective atom relative to the referenced atom. The total energies (ΔE) relative to T_1 are also given, with the total energy of T_1 without SOC set to be zero.

	w/o SOC			w/SOC		
	T_1	H_3	T_4	T_1	H_3	T_4
$d_{\text{Bi-Pb}}$	3.462	3.138	3.149	3.364	3.120	3.145
$d_{\text{Bi-Ge(1)}}$	2.787	3.647	3.635	2.796	3.755	3.803
$d_{\text{Bi-Ge(2)}}$	4.299	4.368	3.586	4.282	4.465	3.769
$d_{\text{Pb-Pb}}$	3.529	3.591	3.588	3.539	3.596	3.590
$d_{\text{Pb-Ge(1)}}$	3.262	2.900	2.899	3.283	2.896	2.897
$\Delta z_{\text{Bi-Pb}}$	0.035	0.013	−0.044	−0.003	0.139	0.171
$\Delta z_{\text{Bi-Ge(1)}}$	2.582	2.801	2.750	2.568	2.929	2.967
$\Delta z_{\text{Pb-Ge(1)}}$	2.547	2.788	2.794	2.571	2.790	2.796
ΔE/eV	0.000	−0.023	0.074	−1.910	−2.037	−1.945

as considerations of other (energetically even more stable) configurations, will be presented in the discussion section.

The three structural models are displayed in Figs. 1(a)–1(c). The structures are first relaxed without SOC, with the structural parameters summarized in Table I. Our DFT calculations without SOC have shown that all these three configurations are confined essentially in single atomic layers, with Bi by 0.035 and 0.013 Å higher than Pb in the T_1 and H_3 configurations, respectively, but by 0.044 Å lower than Pb in the T_4 configuration. In contrast, the results with the inclusion of SOC show that Bi is by 0.003 Å lower than Pb in the T_1 configuration but by 0.139 and 0.171 Å higher than Pb in the H_3 and T_4 configurations, respectively. We also note that the inclusion of SOC has slightly changed the bond lengths and spacings in the z direction, see Table I. Such SOC-induced correction in z can be attributed to the inclusion of the out-of-plane potential gradient which causes a modification to the Born-Oppenheimer energy contour. Similar SOC effect on structural parameters has also been observed in Pb/Si(111) or Pb/Ge(111) [51]. Furthermore, our calculations without and with SOC demonstrate that all three configurations preserve the C_{3v} symmetry, suggesting that the inclusion of the overlayer Bi atoms could be beneficial to the preservation of the structural symmetry.

Next, we investigate the SOC effect on the energetics of the three configurations. We first obtain the energetic profiles without SOC, as listed in Table I. We find that the H_3 structure is more stable than the T_1 and T_4 structures, by 23 and 97 meV per $\sqrt{3}\times\sqrt{3}$ $R30^\circ$ unit cell, respectively. When SOC is included, the H_3 structure is also found to be the most favorable structure among the three configurations, more stable by 127 and 92 meV over the T_1 and T_4 structures, respectively. It is seen that the inclusion of the SOC reverses the relative stability of the T_1 and T_4 structures of Pb_3Bi/Ge(111). In contrast, the SOC has been shown to reverse the relative stability of the H_3 and T_4 for the pure Pb case [51].

Aside from the structural parameters and energetics, it is also desirable to study the degrees of charge transfer between the overlayer and substrate in the three phases, including the

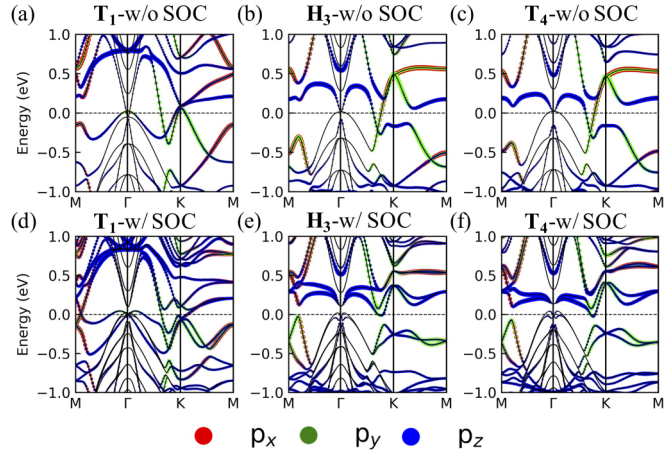

FIG. 2. Band structures of the (a) T_1, (b) H_3, and (c) T_4 configurations calculated without SOC. The corresponding results with SOC are plotted in (d), (e), and (f). Here, the sizes of the red, green, and blue circles denote the spectral weights contributed by the p_x, p_y, and p_z orbitals of the overlayer Pb and Bi atoms, respectively. The Fermi level is set to be zero.

potential influence of the SOC. To this end, we first calculate the charge transfer from the Pb, Bi, and Ge(1) atoms without SOC, all of which are constrained within the surface unit cell as shown by black dashed lines in Fig. 1(a). The results are shown in Fig. S1(a) of the Supplemental Material [52]. For the T_1 phase, there exists comparable charge transfers from the Pb atoms to the neighboring two Ge(1) atoms [labeled as 1 and 3 in Fig. 1(a)] and Bi atoms, due to the similar interatomic distances. In contrast, there exists less charge transfer from the Pb atoms to the Ge(1) atoms [labeled as 2 in Fig. 1(a)] because of the larger interatomic distance. Qualitatively, the directions of charge transfer can be understood by the differences in the atomic electronegativity, given by 1.87, 2.02, and 2.01 for Pb, Bi, and Ge, respectively [53]. As for the H_3 and T_4 phases, the charge transfers from the Pb atoms to the three neighboring Ge(1) atoms and Bi atoms are similar. Furthermore, the charge transfer is more pronounced in the T_1 phase than that of the H_3 and T_4 phases, and such differences in the charge transfer can be manifested by the different band structures of the H_3 or T_4 phases from that of the T_1 phase, as demonstrated in the next subsection. Our detailed calculations also show that the inclusion of the SOC will not change the trends of charge transfer obtained in the absence of SOC but will slightly modify the magnitudes of the charge transfer (see Fig. S1).

B. Electronic structures of the Pb_3Bi/Ge(111) systems

Figures 2(a)–2(c) show the band structures calculated without SOC of the three configurations, together with the projections onto the p_x, p_y, and p_z orbitals of the overlayer atoms (Pb, Bi). It is noticeable that the band structure of the T_1 phase is very different from that of the other two phases. We can see that one hybridized band among the p_x, p_y, and p_z orbitals crosses the Fermi level in T_1 [see Fig. 2(a)], which indicates that these states are part of the bonding states of the Pb_3Bi/Ge(111) interface. Such a significant band hybridization is consistent with the considerable charge transfer from

the surface alloy to the substrate presented above. In contrast, the H_3 and T_4 structures have very similar band dispersions. This behavior can be understood by the comparable charge transfer from the Pb to Ge atoms, and the corresponding structural parameters of these two configurations are close. Furthermore, we find that the projected bands around the Fermi level exhibit strong k dependence within the surface Brillouin zone (SBZ), as reflected by the p_y or p_z orbital along the ΓK line, the p_x or p_z orbital along the ΓM line, and the p_x, p_y, or p_z orbital along the KM line, all of which are shown in Fig. 2(a). Similar behaviors are also displayed in Figs. 2(b) and 2(c).

Next, we examine the effect of SOC on the electronic structures of the three phases, as shown in Figs. 2(d)–2(f). It is found that the degeneracy of the bands has been lifted within the whole SBZ except at the high-symmetry points protected by time-reversal symmetry (i.e., the Γ and M points). When compared with the DFT results without SOC, the DFT+SOC band projections reveal enhanced hybridizations among the p_x, p_y, and p_z orbitals of the overlayer atoms. Specifically, for the T_1 phase, we see clearly that the SOC causes stronger hybridization between the p_y and p_z orbitals along the ΓK line [compare Figs. 2(a) and 2(d)]. For the H_3 phase, we find explicitly that the SOC effectively leads to enhanced hybridization of the p_x and p_z orbitals along the ΓM line, as well as the p_x, p_y, and p_z orbitals along the KM line [see Figs. 2(b) and 2(e)]. For the T_4 phase, the SOC effects on the band structures are similar to that of the H_3 phase [see Figs. 2(c) and 2(f)]. More importantly, it should be emphasized that the SOC induces a significant energy gap of ∼120 and 110 meV along the ΓK line for the H_3 and T_4 phases, respectively, as shown in Figs. 2(e) and 2(f). In contrast, the bands without SOC exhibits Dirac nature, as shown in Figs. 2(b) and 2(c). Such SOC-induced gap openings may lead to topologically nontrivial phase transitions, as elaborated later.

C. Importance of Rashba effects in the $Pb_3Bi/Ge(111)$ systems

In the previous subsections, we have analyzed the overall effects of the SOC on both the atomic and electronic properties of the three phases, without an explicit decomposition of the different physical origins contributing to the SOC. In the present subsection, we focus on the Rashba nature of the SOC, enhanced from the intrinsic components associated with the constituent elements. To identify the asymmetric potential responsible for the Rashba-type SOC and related spin splittings, we plot the in-plane averaged potential along the z direction defined by $V(z) = (\frac{1}{A}) \int V(x, y, z) dx dy$, where A is the area of the $Pb_3Bi/Ge(111)$ surface. The results are shown in Fig. 3, distinctly exhibiting the asymmetric potential within the region of the Pb-Bi overlayer and the first Ge bilayer of the substrate. In contrast, the potential is largely symmetric in the deeper layers of the substrate. These behaviors indicate that the local asymmetric potential induces Rashba SOC and spin splitting mainly in the Pb-Bi overlayer and the first Ge bilayer of the substrate. Additionally, for each of the three phases, we note that there is an abrupt change in the plane-averaged potential at about 27 Å in the repeated-slab calculations. Such behaviors can be attributed to the different work functions of the upper and lower surfaces associated with the asymmetric

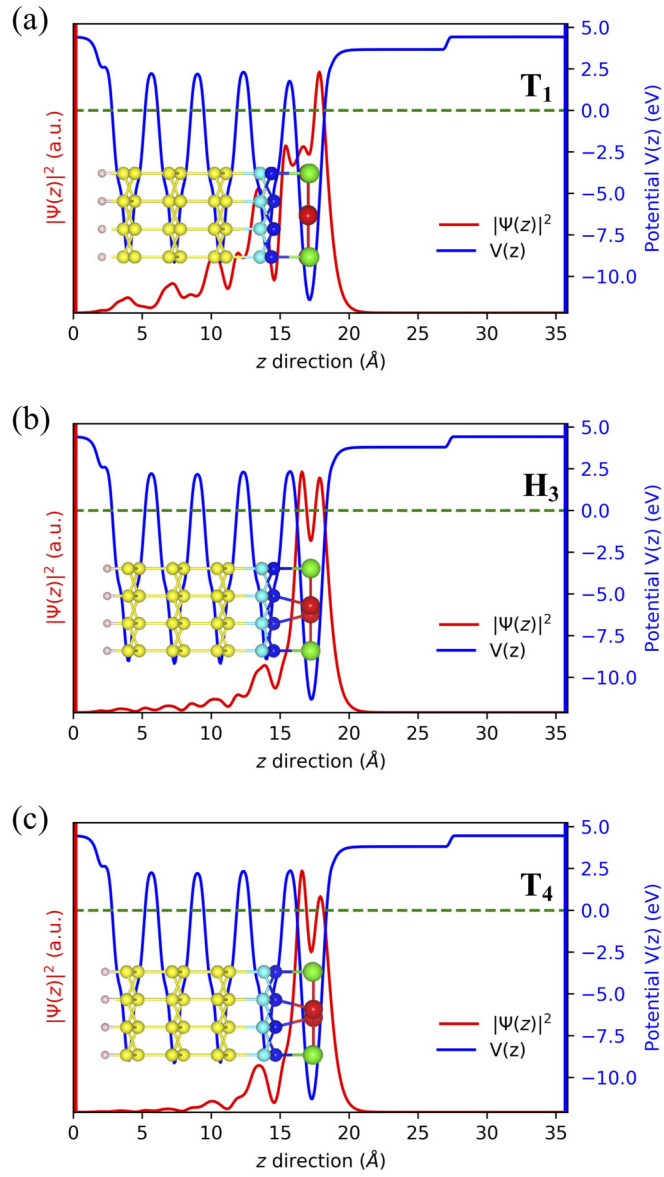

FIG. 3. Distributions of the screening electron density $|\Psi(z)|^2$ in the vicinity of the Fermi level and the plane-averaged potential $V(z)$ along the z axis of the (a) T_1, (b) H_3, and (c) T_4 configurations. The corresponding atomic positions are also superposed onto the potential energy curves. The Fermi level is set to be zero.

slab model systems. Such abrupt changes can be viewed as dipole layers in the DFT calculations for slab systems, and the two sides are the vacuum levels for the two surfaces. The electron density distributions $|\Psi(z)|^2$ obtained by integrating within the window of [E_F −0.1 eV, E_F +0.1 eV] also confirm that the screening charge is mostly distributed within the Pb-Bi overlayer and the first Ge bilayer of the substrate, while it is almost negligibly small in the deeper layers (see Fig. 3).

To get a deeper understanding of the spin splittings in the electron bands, we further analyze the characteristics of the band projection onto the S_x, S_y, and S_z components of the total spin vector defined by $|S| = \sqrt{S_x^2 + S_y^2 + S_z^2}$. Figures 4(a)–4(f) illustrate the S_x and S_y spin components, as highlighted by the different colored dots (blue and red for S_x, orange and purple

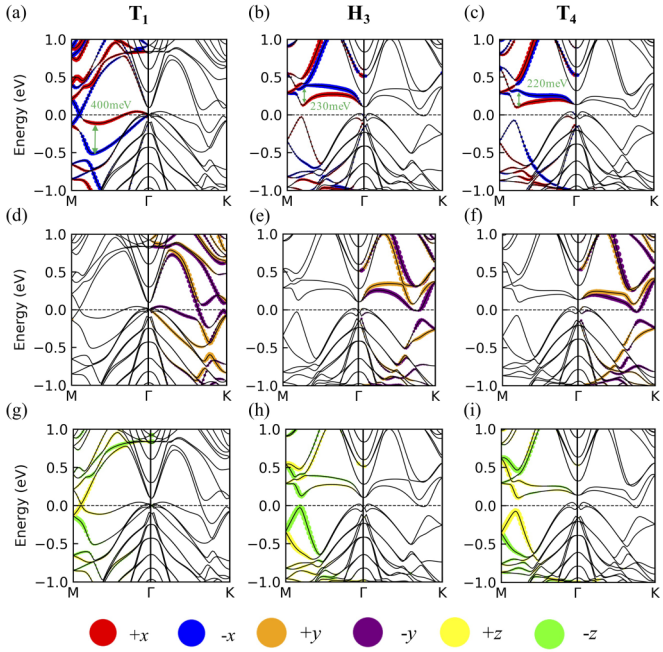

FIG. 4. Band structures in-plane projected onto the S_x spin components of the Pb-Bi overlayer for the (a) T_1, (b) H_3, and (c) T_4 configurations calculated with SOC. The sizes of the blue and red circles indicate the spectral weights contributed by the opposite S_x spin components. (d)–(f) The corresponding S_y spin component projections. The sizes of the orange and purple circles indicate the spectral weights contributed by the opposite S_y spin components. (g)–(i) The corresponding out-of-plane projected S_z spin components, with the sizes of the green and yellow circles indicating the spectral weights contributed by the opposite spin components. The Fermi level is set to be zero.

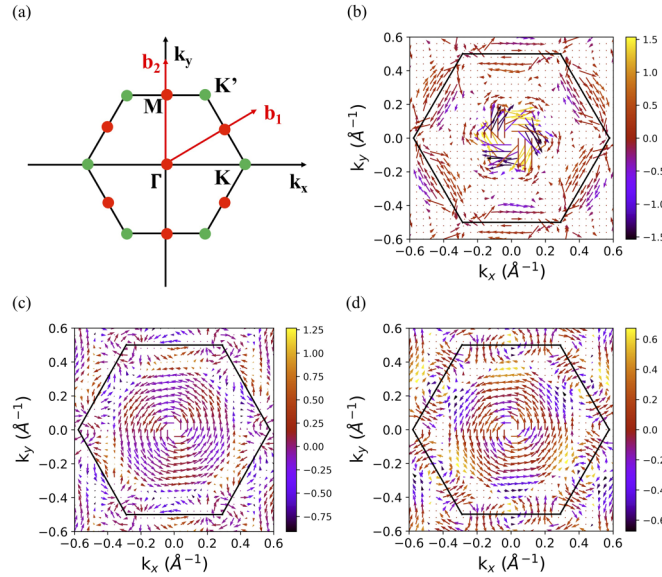

FIG. 5. (a) Surface Brillouin zone (SBZ) of the $Pb_3Bi/Ge(111)$ systems. The red and green solid circles indicate the k points with and without time-reversal symmetry, respectively. (b)–(d) Calculated spin textures of the upper branches of the spin-split surface bands shown in Fig. 4 for the T_1, H_3, and T_4 configurations, respectively. The lengths of the arrows scale with the magnitudes of the in-plane spin components. The values of the out-plane spin components are depicted by the color bars, where the "+" and "−" values represent the upward and downward spin directions, respectively.

for S_x). Here we unambiguously reveal the Rashba nature of the band splitting. As shown in Fig. S2, the two Rashba spin-split surface bands along the M → Γ →−M path in the momentum space for the T_1 phase typically have the "+x" and "−x" spin polarizations but no y components, since the ΓM line is parallel to the y axis. Similarly, for the K′→ Γ → K path, which is parallel to the x axis, the two spin-split surface bands only host the "+y" and "−y" spin polarizations but no x components, as shown in Fig. S3. Similar Rashba features in the H_3 and T_4 phases are also displayed in Figs. S4–S7. Here we unambiguously reveal the Rashba nature of the band splittings. Specifically, the T_1 phase has a very large spin splitting of 400 meV along the ΓM line below the Fermi level [see Fig. 4(a)], which is even larger than the previously reported value of 250 meV in the 2D superconductor of Tl-Pb on Si(111) [26,27]. The further enhanced spin splitting in the present system may be attributed to the stronger atomic SOC of Bi than Tl. Such giant Rashba splittings have also been observed in the H_3 and T_4 phases, given by 230 and 220 meV along the ΓM line above the Fermi level, respectively [as shown in Figs. 4(b) and 4(c)]. Furthermore, from Figs. 4(g)–4(i), the S_z spin component is only distributed in the vicinity of the M point along the ΓM line. A finite S_z spin component on the ΓM line can be explained by symmetry considerations within the momentum space, as given below. In the direction parallel to the z axis, there exist mirror planes along the ΓK and MK lines in the SBZ, while no such mirror symmetry exists along the ΓM line [see Fig. 5(a)]. Therefore, any S_z spin component inside the mirror plane is quenched upon a mirror symmetry operation, consistent with the observation that no S_z spin component exists along the ΓK line in Figs. 4(g)–4(i). However, such a constraint is lacking along the ΓM line; accordingly, a finite S_z spin component is present along the ΓM line, as shown in Figs. 4(g)–4(i).

From Fig. 5(a), we also see that there are three mirror planes crossing the Γ and K points but only one mirror plane crossing the M point. Such different symmetries between the high-symmetry points can induce intriguing spin textures. Figures 5(b)–5(d) show the helical spin textures of the contour over the whole SBZ, as displayed by the in-plane and out-of-plane spin components of the upper branch of the surface states. We can see that the spin vector directions rotate for all the three phases. We also note that, in Fig. 5(b), the anisotropic Rashba spin splittings take place around the six M points, which can be explained by the existence of the C_{1h} symmetry at the M points [54,55]. Such helical spin structure surrounding the center of the SBZ explicitly indicates the characteristic feature of the Rashba effect. We have also demonstrated above that each of the three phases preserves the C_{3v} symmetry; therefore, the out-of-plane spin component oscillates between the positive and negative values at the Fermi level [27]. Moreover, we note that, for the T_1 phase, the maximum of the electron density is located on the vacuum side. In contrast, the maximum of the electron density for either the H_3 or T_4 phase is located on the substrate side.

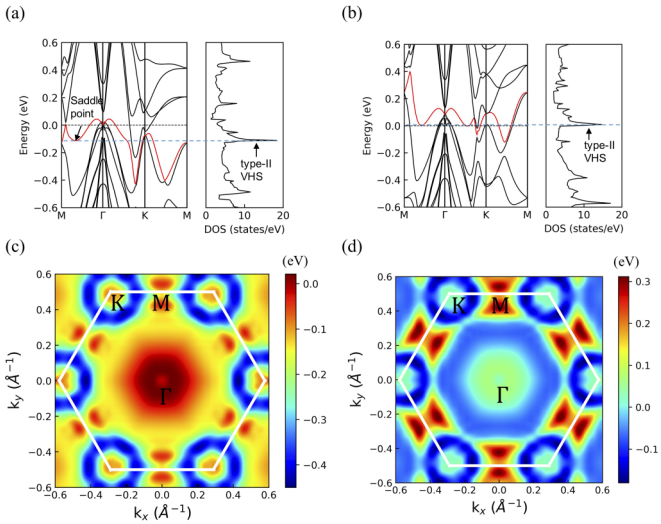

FIG. 6. Band structures and densities of states of (a) Pb_3Bi and (b) pure Pb on the Ge(111) substrate, both in the T_1 configuration. The surface states in the vicinity of the Fermi level are highlighted by the red lines, and the corresponding contours are displayed in (c) and (d). The edges of the SBZ in (c) and (d) are indicated by the white solid lines. The Fermi level is set to be zero.

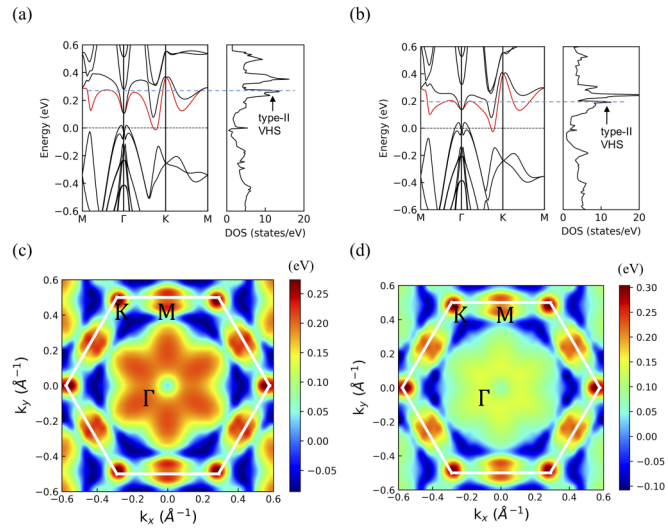

FIG. 7. Band structures and densities of states of the Pb_3Bi/Ge(111) systems in the (a) H_3 and (b) T_4 configurations. The surface states are highlighted by the red lines, and the corresponding contours are displayed in (c) and (d). The edges of the SBZ in (c) and (d) are indicated by the white solid lines. The Fermi level is set to be zero.

Such differences in the electronic density distributions may be responsible for the reversal of the spin orientations of the surface states between the T_1 and the H_3 (or T_4) phase [see Figs. 4(a)–4(c)] [56,57]. These intriguing spin textures serve as indispensable ingredients to the emergence of nontrivial topology, as shown for the T_1 phase previously [33], and also for the other two phases in a later subsection.

D. Van Hove singularity in the Pb_3Bi/Ge(111) systems

In 2D systems, a saddlelike band dispersion may lead to a logarithmic divergence in the density of states (DOS), known as the VHS. As a counterpart, an extremum of a paraboliclike band dispersion may result in a 1D-like square-root singularity in the DOS [58,59]. The prominent role of the VHS in strongly correlated phenomena has been emphasized extensively [60–62]. The resulting intriguing phases may include charge density wave [63] and chiral or topological superconductivity [33,34,64]. Recently, the VHS has been further classified into two types [64]. The type-I VHS is originated from the saddle points where the time-reversal symmetry is invariant. In such systems, the topologically nontrivial superconductivity with triplet pairing would be suppressed because of its odd parity. However, the type-II VHS, derived from the saddle points without the protection of time-reversal symmetry, can host topological superconductivity by proper doping [33,64]. Such conceptual advances motivate the present study of materials specific systems that may harbor type-II VHS.

For the system of Pb_3Bi/Ge(111), we have demonstrated that the existence of the type-II VHS together with geometric phase may result in chiral topological superconductivity in the T_1 phase [33]. Figure 6(a) shows the position of the type-II VHS and corresponding saddlelike band structure. As shown in Fig. 6(c), the contour along the ΓM line first goes downward, then goes upward. Meanwhile, the contour along the $k_x \sim 0.35$ Å^{-1} line first goes up to the maximal value, then goes down. Together, such dispersion features characterize the saddle point in the band structure. The calculated DOS in Fig. 6(a) also shows a divergent trend below the Fermi level, further confirming the emergence of the type-II VHS.

To elucidate the important role of the doped Bi atoms in the formation of the saddlelike band dispersion and corresponding type-II VHS, we consider a pure Pb overlayer constrained in the T_1 phase. The corresponding band structure with the inclusion of the SOC is shown in Fig. 6(b), which is similar to that of Pb_3Bi/Ge(111), but shifted upwards. This behavior can be understood by the fewer valence electrons in the pure Pb system. Furthermore, we find that the DOS exhibits a 1D-like square-root singularity near the Fermi level, mainly contributed from the band extremum region [see Fig. 6(d)]. Such a sharp DOS at the Fermi level is more likely to drive a structural instability [63] in the T_1 phase of the pure Pb overlayer. Given that the T_1 phase of Pb/Ge(111) or Pb/Si(111) by now has not been observed experimentally [47–50], we suspect that such instabilities might be responsible for its absence in the existing experimental studies. In this regard, the Bi doping not only alters the nature of the type-II VHS, but also may help to stabilize the T_1 phase, as the corresponding VHS is now noticeably below the Fermi level.

Next, we explore the potential existence of VHS in the H_3 and T_4 phases. Figures 7(a) and 7(b) explicitly display a sharp DOS at ∼0.3 and 0.2 eV above the Fermi level for the H_3 and T_4 phases, respectively. Furthermore, from either Fig. 7(c) or Fig. 7(d), we identify the existence of a band extremum along the ΓM line, as well as a saddle point along the ΓK line. Therefore, the existence of the sharp DOS can be attributed to the joint result of the band extremum of the largely parabolic

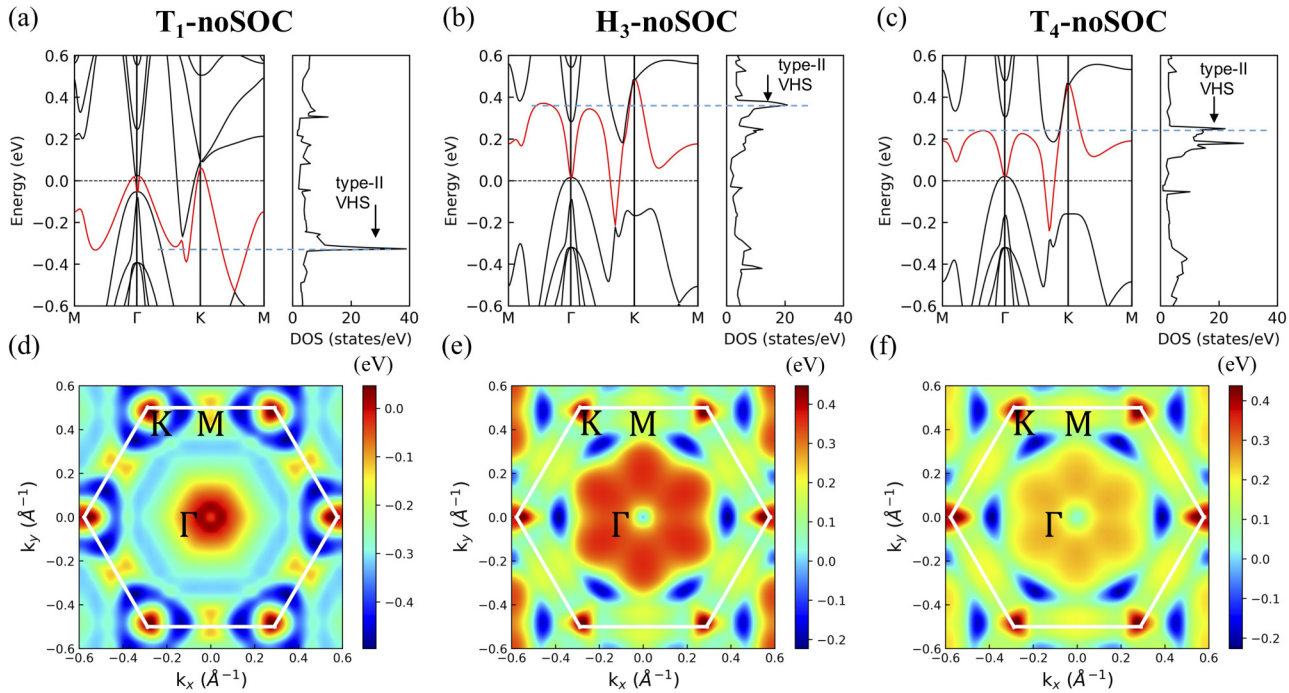

FIG. 8. Band structures and densities of states of the Pb_3Bi/Ge(111) system in the (a) T_1, (b) H_3, and (c) T_4 configurations obtained in the absence of SOC. The surface states are highlighted by the red lines, and the corresponding contours are displayed in (d), (e), and (f). The edges of the SBZ in (d), (e), and (f) are indicated by the white solid lines. The Fermi level is set to be zero.

band structure and the saddlelike band structure, leading to the emergence of the type-II VHS.

It is also worthwhile to highlight the important role of the SOC in the existence and in particular the location of the VHS for each of the three phases. In doing so, we calculate the corresponding electronic structures in the absence of SOC, as shown in Figs. 8(a)–8(c). We notice that, even without SOC, the divergent DOS is present for each phase as well, but its location is far away from the Fermi level. Therefore, the Rashba enhanced SOC plays a vital role in tuning the location of the VHS to experimentally accessible regions.

E. Topological properties of the Pb_3Bi/Ge(111) systems

In our previous work [33], we have employed a functional renormalization group method to study the interplay between geometric phase and electron correlation. In this approach, all the competing orders such as superconductivity, charge density wave, spin density wave, and nematicity can be treated on an equal footing. The central findings are that the renormalized geometric phase flows to three stable fixed points, not only favoring the realization of intrinsically topological chiral *p*-wave or *f*-wave superconductivity, but also enhancing the corresponding superconducting order. Using first-principles calculations, we have further predicted that the hole-doped Pb_3Bi grown on Ge(111) surface (namely, the T_1 phase) is a 2D topological superconducting system.

In the present study, we expand our effort by carrying out a comparative study of the topological properties of all three phases. First, due to the heavy hybridization between the overlayer and Ge substrate [see Figs. 2(e) and 2(f)], the wannierlization process [45] adopted to evaluate the topological properties requires projections onto the *p* orbitals of not only the overlayer but also the whole Ge substrate. Such an exercise will drastically increase the dimensionality of the projection basis, leading to demanding technical difficulty. To mitigate this issue, we downfold the projection basis to a subspace spanned by only the *p* orbitals of the Pb-Bi overlayer and topmost Ge bilayer. Such an approximation is reasonable, because the hybridization between the Pb, Bi, and Ge atoms beneath the Ge bilayer decays rapidly, as also demonstrated by the screening charge distribution shown in Fig. 3. We then simplify the model systems by using one Ge bilayer to simulate the Ge(111) substrate, and the calculated band structures of the H_3 and T_4 phases are shown in Figs. 9(a) and 9(c), respectively. Our PBE+SOC calculations indeed confirm that the simplification did not change the main features of the band structures when compared with that of the systems with a thicker Ge substrate [see Figs. 2(e) and 2(f)]. Importantly, we find that each of the H_3 and T_4 structures hosts a topologically nontrivial phase with $Z_2 = 1$, characterized by a quantum spin Hall state. To further illustrate the nontrivial topology of the H_3 and T_4 phases within the PEB+SOC scheme, we now calculate the band structures by employing the hybrid functionals [42], which are expected to better describe the band gaps. The corresponding band structures within the HSE06 are displayed in Figs. 9(a) and 9(c), showing full band gaps of 25 and 50 meV, respectively. The calculated Z_2 invariant remains to be 1 for both systems, preserving the nontrivial topology.

As another manifestation of the nontrivial topology in the band structures, we further obtain the edge states of the H_3 and T_4 phases using the HSE06 results and semi-infinite lattice models [44]. The results are shown in Figs. 9(b) and 9(d) for the H_3 and T_4 structures, respectively, highlighting the

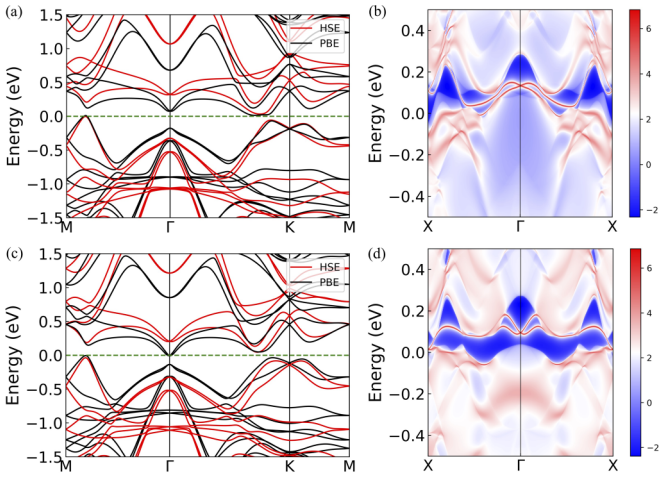

FIG. 9. Band structures obtained using the PBE+SOC and HSE06+SOC schemes for the (a) H_3 and (c) T_4 configurations. One Ge bilayer is used to model the substrate, as justified in the main text. The corresponding spectra of the semi-infinite slabs with a Pb-Bi edge along the x direction are displayed in (b) and (d). The Fermi level is set to be zero.

Dirac-like nature of the edge states near the Fermi level. Given the existence of robust topological states demonstrated here and the experimentally accessible type-II VHS presented earlier, we expect that the H_3 and T_4 structures could not only host quantum spin Hall states but may also harbor topological superconductivity upon proper doping [33,65–67].

IV. DISCUSSIONS

Two-dimensional electron systems with giant Rashba splittings have been attractive in the area of topological materials [68,69], because the corresponding significant SOC strengths may serve as a pivotal physical factor in inducing topological states of matter. As one compelling example, it has been recently demonstrated that a quantum spin Hall state can be triggered in the Rashba system of bismuthene/SiC(0001) [70]. As related developments, a WTe_2 monolayer has been shown to be able to harbor a quantum spin Hall state [65] or superconductivity under proper conditions [66,67]. More recently, the T_1 phase has also been shown as a platform to realize chiral topological superconductivity [33]. Given these exciting developments, it remains desirable and potentially rewarding to search for new candidate platforms that can host intriguing topological or collective properties based on Rashba systems. At a concrete level, the results gained in the present work may serve as the basis for realization of the above expectations. In particular, we have shown the existence of the VHS in the H_3 and T_4 phases, which have been induced by the Bi doping. When further electron doped, for example at proper gating conditions, the H_3 and T_4 phases might host odd-parity superconductivity [33,64].

Beyond the three high-symmetry phases studied so far, we have also performed more relaxed structural search by placing the Bi atoms on the low-symmetry positions, generating 24 initial candidate structures. After structural optimization, we find two other energetically degenerate configurations labeled

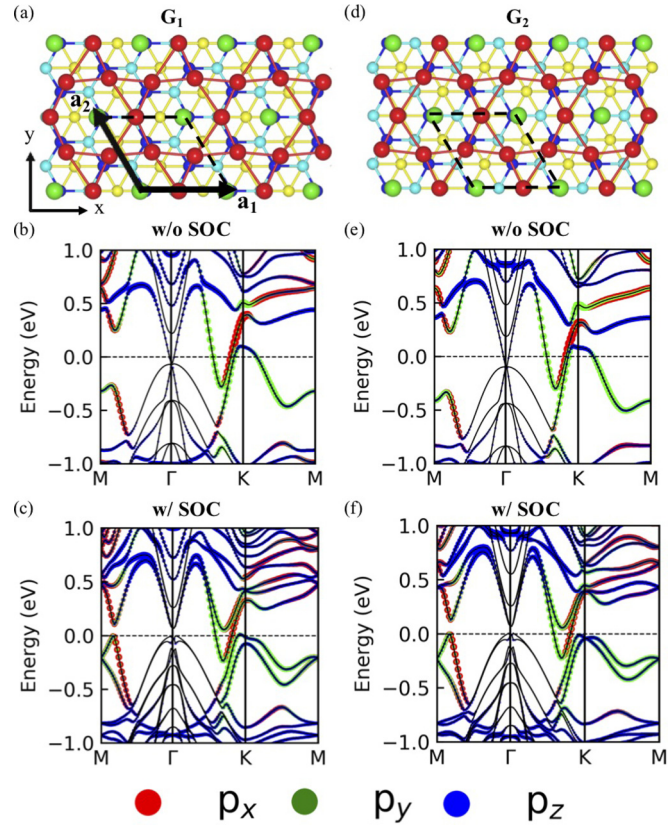

FIG. 10. Top views of the Pb_3Bi/Ge(111) system in the (a) G_1 and (d) G_2 configurations, where the unit cells are highlighted by the black dashed lines. Band structures of (b) G_1 and (e) G_2 configurations calculated without SOC, with the corresponding SOC results plotted in (c) and (f). Here, the sizes of the red, green, and blue circles denote the spectral weights contributed by the p_x, p_y, and p_z orbitals of the overlayer (Pb plus Bi) atoms, respectively. The Fermi level is set to be zero.

as G_1 and G_2 [see Figs. 10(a) and 10(d)]. Their total energies are lower by ~0.2 eV per $\sqrt{3}\times\sqrt{3}$ $R30^\circ$ substrate supercell. The band structures of the two phases without and with SOC are displayed in Fig. 10. By examining the detailed band structures, we observe clear spin splittings with the inclusion of the SOC but no gap opening in either of the two configurations. To reveal the topology of these two phases, we apply the same method as used for the H_3 and T_4 phases above. The PBE+SOC and HSE06+SOC band structures of the G_1 and G_2 phases with one Ge bilayer in the substrate are shown in Figs. S8(a) and S8(b), respectively. Though there is no global gap, we can identify a curved "gap" to calculate the Z_2 invariant for all the states below this curved "gap." By using the Wannier charge center method implemented in the WannierTools package, the corresponding Z_2 is calculated to be zero for either of the G_1 and G_2 configurations, indicating their trivial topological nature. Such behaviors are also the very reason that our study has been primarily focused on the metastable but topologically nontrivial T_1, H_3, and T_4 phases. These observations are consistent with the results of existing studies. For example, the metastable transition metal dichalcogenides have been theoretically proposed and experimentally verified to exhibit quantum spin Hall phase [71–73],

while the more stable 2H phase is trivial [74–76]. The underlying rationale can be attributed to the delicate competition between the crystal field and SOC effects [77].

Before closing, we briefly discuss the growth aspects of the Pb-Bi thin films on the Ge substrate. Given the specific atomic configurations of the Pb_3Bi alloy, one may grow a pristine Pb film at a proper coverage first, then deposit additional Bi atoms onto the Pb/Ge(111) system, as demonstrated in the growth of Tl-Pb compound on Si(111) [26,27]. Physical realizations of the proposed systems may further lead to definitive validations of the strong and intriguing predictions made in this work.

V. CONCLUSIONS

In summary, we have systematically investigated the structural, electronic, and topological properties of the Pb_3Bi alloy grown on the Ge(111) substrate. We first identified the existence of three distinct phases, labeled as T_1, H_3, and T_4, which are of high symmetry and energetically nearly degenerate. All the three phases have been shown to possess giant Rashba enhanced SOC and corresponding spin splittings. Next, we showed that each of the saddle- and paraboliclike band dispersions can result in the emergence of type-II Van Hove singularity, whose positions can be substantially tuned by the giant Rashba effects to the vicinity of the Fermi level. More importantly, we identified the presence of topological states hosted by both the H_3 and T_4 structures, with the openings of topologically nontrivial gaps of 25 and 50 meV, respectively. Given the energetic affinity of the three phases, our findings point to the feasibility of realizing quantum phase transitions between quantum spin Hall effect and topological superconductivity within the same materials platform. The present study is expected to give new insights in searching for topological quantum states including 2D topological superconductivity based on Rashba systems.

ACKNOWLEDGMENTS

We thank Prof. Jun-Hyung Cho for helpful discussions in the initial stage of this work. This work was supported by the National Key R&D Program of China (Grant No. 2017YFA0303500), the National Natural Science Foundation of China (Grants No. 11634011, No. 11722435, No. 11974323, and No. 11904350), the Anhui Initiative in Quantum Information Technologies (Grant No. AHY170000), and the Strategic Priority Research Program of Chinese Academy of Sciences (Grant No. XDB30000000).

[1] Y. A. Bychkov and E. I. Rashba, JETP Lett. **39**, 78 (1984).
[2] S. LaShell, B. A. McDougall, and E. Jensen, Phys. Rev. Lett. **77**, 3419 (1996).
[3] J. Nitta, T. Akazaki, H. Takayanagi, and T. Enoki, Phys. Rev. Lett. **78**, 1335 (1997).
[4] A. Manchon, H. C. Koo, J. Nitta, S. M. Frolov, and R. A. Duine, Nat. Mater. **14**, 871 (2015).
[5] L. Petersen and P. Hedegard, Surf. Sci. **459**, 49 (2000).
[6] Y. M. Koroteev, G. Bihlmayer, J. E. Gayone, E. V. Chulkov, S. Blugel, P. M. Echenique, and Ph. Hofmann, Phys. Rev. Lett. **93**, 046403 (2004).
[7] B. Fluegel, S. Francoeur, A. Mascarenhas, S. Tixier, E. C. Young, and T. Tiedje, Phys. Rev. Lett. **97**, 067205 (2006).
[8] I. Gierz, T. Suzuki, E. Frantzeskakis, S. Pons, S. Ostanin, A. Ernst, J. Henk, M. Grioni, K. Kern, and C. R. Ast, Phys. Rev. Lett. **103**, 046803 (2009).
[9] F. A. Zwanenburg, A. S. Dzurak, A. Morello, M. Y. Simmons, L. C. L. Hollenberg, G. Klimeck, S. Rogge, S. N. Coppersmith, and M. A. Eriksson, Rev. Mod. Phys. **85**, 961 (2013).
[10] C. R. Ast, J. Henk, A. Ernst, L. Moreschini, M. C. Falub, D. Pacile, P. Bruno, K. Kern, and M. Grioni, Phys. Rev. Lett. **98**, 186807 (2007).
[11] K. Yaji, Y. Ohtsubo, S. Hatta, H. Okuyama, K. Miyamoto, T. Okuda, A. Kimura, H. Namatame, M. Taniguchi, and T. Aruga, Nat. Commun. **1**, 17 (2010).
[12] L. Fu and C. L. Kane, Phys. Rev. Lett. **100**, 096407 (2008).
[13] M. Sato and S. Fujimoto, Phys. Rev. B **79**, 094504 (2009).
[14] J. D. Sau, R. M. Lutchyn, S. Tewari, and S. Das Sarma, Phys. Rev. Lett. **104**, 040502 (2010).
[15] R. M. Lutchyn, J. D. Sau, and S. Das Sarma, Phys. Rev. Lett. **105**, 077001 (2010).
[16] M.-X. Wang, C. Liu, J.-P. Xu, F. Yang, L. Miao, M.-Y. Yao, C. L. Gao, C. Shen, X. Ma, X. Chen, Z.-A. Xu, Y. Liu, S.-C. Zhang, D. Qian, J.-F. Jia, and Q.-K. Xue, Science **336**, 52 (2012).
[17] V. Mourik, K. Zuo, S. M. Frolov, S. R. Plissard, E. P. A. M. Bakkers, and L. P. Kouwenhoven, Science **336**, 1003 (2012).
[18] C. Nayak, S. H. Simon, A. Stern, M. Freedman, and S. Das Sarma, Rev. Mod. Phys. **80**, 1083 (2008).
[19] J. Alicea, Rep. Prog. Phys. **75**, 076501 (2012).
[20] M. Sato and Y. Ando, Rep. Prog. Phys. **80**, 076501 (2017).
[21] V. Yeh, L. Berbil-Bautista, C. Z. Wang, K. M. Ho, and M. C. Tringides, Phys. Rev. Lett. **85**, 5158 (2000).
[22] J. H. Dil, F. Meier, J. Lobo-Checa, L. Patthey, G. Bihlmayer, and J. Osterwalder, Phys. Rev. Lett. **101**, 266802 (2008).
[23] M. M. Özer, Y. Jia, Z. Y. Zhang, J. R. Thompson, and H. H. Weitering, Science **316**, 1594 (2007).
[24] F. Meier, V. Petrov, S. Guerrero, C. Mudry, L. Patthey, J. Osterwalder, and J. H. Dil, Phys. Rev. B **79**, 241408(R) (2009).
[25] Y. Jia, S. Y. Wang, W. G. Chen, Q. Sun, H. H. Weitering, and Z. Y. Zhang, Phys. Rev. B **81**, 245425 (2010)
[26] D. V. Gruznev, L. V. Bondarenko, A. V. Matetskiy, A. A. Yakovlev, A. Y. Tupchaya, S. V. Eremeev, E. V. Chulkov, J. P. Chou, C. M. Wei, M. Y. Lai, Y. L. Wang, A. V. Zotov, and A. A. Saranin, Sci. Rep. **4**, 4742 (2014).
[27] A. V. Matetskiy, S. Ichinokura, L. V. Bondarenko, A. Y. Tupchaya, D. V. Gruznev, A. V. Zotov, A. A. Saranin, R. Hobara, A. Takayama, and S. Hasegawa, Phys. Rev. Lett. **115**, 147003 (2015).
[28] Y. Guo, Y.-F. Zhang, X.-Y. Bao, T.-Z. Han, Z. Tang, L.-X. Zhang, W.-G. Zhu, E. G. Wang, Q. Niu, Z. Q. Qiu, J.-F. Jia, Z.-X. Zhao, and Q.-K. Xue, Science **306**, 1915 (2004).
[29] S. Qin, J. Kim, Q. Niu, and C.-K. Shih, Science **324**, 1314 (2009).
[30] T. Zhang, P. Cheng, W.-J. Li, Y.-J. Sun, G. Wang, X.-G. Zhu, K. He, L. Wang, X. Ma, X. Chen, Y. Wang, Y. Liu, H.-Q. Lin, J.-F. Jia, and Q.-K. Xue, Nat. Phys. **6**, 104 (2010).

[31] C. Brun, T. Cren, V. Cherkez, F. Debontridder, S. Pons, D. Fokin, M. C. Tringides, S. Bozhko, L. B. Ioffe, B. L. Altshuler, and D. Roditchev, Nat. Phys. **10**, 104 (2014).

[32] H. Nama, H. Chen, T. Liu, J. Kim, C. Zhang, J. Yong, T. R. Lemberger, P. A. Kratz, J. R. Kirtley, K. Moler, P. W. Adams, A. H. MacDonald, and C.-K. Shih, Proc. Natl. Acad. Sci. USA **113**, 10513 (2016).

[33] W. Qin, L. Li, and Z. Y. Zhang, Nat. Phys. **15**, 796 (2019).

[34] R. Nandkishore, L. S. Levitov, and A. V. Chubukov, Nat. Phys. **8**, 158 (2012).

[35] Y. Cao, Y. Fatemi, S. Fang, K. Watanabe, T. Taniguchi, E. Kaxiras, and P. Jarillo-Herrero, Nature (London) **556**, 43 (2018).

[36] G. Kresse and J. Furthmüller, Phys. Rev. B **54**, 11169 (1996).

[37] G. Kresse and J. Hafner, Phys. Rev. B **48**, 13115 (1993).

[38] P. E. Blöchl, Phys. Rev. B **50**, 17953 (1994).

[39] G. Kresse and D. Joubert, Phys. Rev. B **59**, 1758 (1999).

[40] J. P. Perdew, K. Burke, and M. Ernzerhof, Phys. Rev. Lett. **77**, 3865 (1996).

[41] S. Grimme, J. Antony, S. Ehrlich, and S. Krieg, J. Chem. Phys. **132**, 154104 (2010).

[42] J. Heyd, G. E. Scuseria, and M. J. Ernzerhof, J. Chem. Phys. **118**, 8207 (2003).

[43] A. A. Soluyanov and D. Vanderbilt, Phys. Rev. B **83**, 235401 (2011).

[44] M. P. L. Sancho, J. M. L. Sancho, J. M. L. Sancho, and J. Rubio, Phys. F: Met. Phys. **15**, 851 (1985).

[45] A. A. Mostofi, J. R. Yates, Y.-S. Lee, I. Souza, D. Vanderbilt, and N. Marzari, Comput. Phys. Commun. **178**, 685 (2008).

[46] Q. Wu, S. Zhang, H.-F. Song, M. Troyer, and A. A. Soluyanov, Comput. Phys. Commun. **224**, 405 (2018).

[47] H. Huang, C. M. Wei, H. Li, B. P. Tonner, and S. Y. Tong, Phys. Rev. Lett. **62**, 559 (1989).

[48] L. Seehofer, G. Falkenberg, D. Daboul, and R. L. Johnson, Phys. Rev. B **51**, 13503 (1995).

[49] K. Horikoshi, X. Tong, T. Nagao, and S. Hasegawa, Phys. Rev. B **60**, 13287 (1999).

[50] T. L. Chan, C. Z. Wang, M. Hupalo, M. C. Tringides, Z.-Y. Lu, and K. M. Ho, Phys. Rev. B **68**, 045410 (2003).

[51] X.-Y. Ren, H.-J. Kim, S. Yi, Y. Jia, and J.-H. Cho, Phys. Rev. B **94**, 075436 (2016).

[52] See Supplemental Material at http://link.aps.org/supplemental/10.1103/PhysRevB.102.035150 for the illustration of (i) charge transfer from the Pb, Bi, and Ge(1) atoms in the T_1, H_3, and T_4 configurations; (ii) band structures projected on the in-plane spin components of the T_1, H_3, and T_4 configurations; (iii) the PBE+SOC and HSE06+SOC band structures of the G_1 and G_2 phases with one Ge bilayer substrate.

[53] L. Pauling, J. Am. Chem. Soc **54**, 3570 (1932).

[54] T. Oguchi and T. Shishidou, J. Phys.: Condens. Mater **21**, 092001 (2009).

[55] K. Sakamoto, H. Kakuta, K. Sugawara, K. Miyamoto, A. Kimura, T. Kuzumaki, N. Ueno, E. Annese, J. Fujii, A. Kodama, T. Shishidou, H. Namatame, M. Taniguchi, T. Sato, T. Takahashi, and T. Oguchi, Phys. Rev. Lett. **103**, 156801 (2009).

[56] M. Nagano, A. Kodama, T. Shishidou, and T. Oguchi, J. Phys.: Condens. Mater **21**, 064239 (2009).

[57] H. Bentmann, T. Kuzumaki, G. Bihlmayer, S. Blügel, E. V. Chulkov, F. Reinert, and K. Sakamoto, Phys. Rev. B **84**, 115426 (2011).

[58] E. Cappelluti, C. Grimaldi, and F. Marsiglio, Phys. Rev. Lett. **98**, 167002 (2007).

[59] T. Cao, Z. Li, and S. G. Louie, Phys. Rev. Lett. **114**, 236602 (2015).

[60] N. Furukawa, T. M. Rice, and M. Salmhofer, Phys. Rev. Lett. **81**, 3195 (1998).

[61] C. Honerkamp and M. Salmhofer, Phys. Rev. Lett. **87**, 187004 (2001).

[62] T. Hänke, S. Sykora, R. Schlegel, D. Baumann, L. Harnagea, S. Wurmehl, M. Daghofer, B. Büchner, J. van den Brink, and C. Hess, Phys. Rev. Lett. **108**, 127001 (2012).

[63] J. González, Phys. Rev. B **62**, 6928 (2000).

[64] H. Yao and F. Yang, Phys. Rev. B **92**, 035132 (2015).

[65] S. Wu, V. Fatemi, Q. D. Gibson, K. Watanabe, T. Taniguchi, R. J. Cava, and P. Jarillo-Herrero, Science **359**, 76 (2018).

[66] E. Sajadi, T. Palomaki, Z. Fei, W. Zhao, P. Bement, C. Olsen, S. Luescher, X. Xu, J. A. Fork, and D. H. Cobden, Science **362**, 922 (2018).

[67] V. Fatemi, S. Wu, Y. Cao, L. Bretheau, Q. D. Gibson, K. Watanabe, T. Taniguchi, R. J. Cava, and P. Jarillo-Herrero, Science **362**, 926 (2018).

[68] M. Z. Hasan and C. L. Kane, Rev. Mod. Phys. **82**, 3045 (2010).

[69] X.-L. Qi and S.-C. Zhang, Rev. Mod. Phys. **83**, 1057 (2011).

[70] F. Reis, G. Li, L. Dudy, M. Bauernfeind, S. Glass, W. Hanke, R. Thomale, J. Schäfer, and R. Claessen, Science **357**, 287 (2017).

[71] X. Qian, J. Liu, L. Fu, and J. Li, Science **346**, 1344 (2014).

[72] P. Chen, W. W. Pai, Y.-H. Chan, W.-L. Sun, C.-Z. Xu, D.-S. Lin, M. Y. Chou, A.-V. Fedorov, and T.-C. Chiang, Nat. Commun. **9**, 2003 (2018).

[73] M. M. Ugeda, A. Pulkin, S. Tang, H. Ryu, Q. Wu, Y. Zhang, D. Wong, Z. Pedramrazi, A. Martín-Recio, Y. Chen, F. Wang, Z.-X. Shen, S.-K. Mo, O. V. Yazyev, and M. F. Crommie, Nat. Commun. **9**, 3401 (2018).

[74] T. Zhang, Y. Jiang, Z. Song, H. Huang, Y. He, Z. Fang, H. Weng, and C. Fang, Nature (London) **566**, 475 (2019).

[75] M. G. Vergniory, L. Elcoro, C. Felser, N. Regnault, B. Andrei Bernevig, and Z. Wang, Nature (London) **566**, 480 (2019).

[76] F. Tang, H. C. Po, A. Vishwanath, and X. Wan, Nature (London) **566**, 486 (2019).

[77] G. Cao, H. Liu, X.-Q. Chen, Y. Sun, J. Liang, R. Yu, and Z. Y. Zhang, Sci. Bull. **62**, 1649 (2017).

Supplemental Material for

Emergence of van Hove singularity and topological states in Pb_3Bi/Ge(111) Rashba systems

Leiqiang Li,[1] Shang Ren[1,*], Wei Qin,[1,2] Shunhong Zhang[1], Xiangang Wan[3], Yu Jia[4], Ping Cui,[1,5,†] and Zhenyu Zhang[1,†]

[1]*International Center for Quantum Design of Functional Materials (ICQD), Hefei National Laboratory for Physical Sciences at the Microscale, and CAS Center for Excellence in Quantum Information and Quantum Physics, University of Science and Technology of China, Hefei, Anhui 230026, China*

[2]*Department of Physics, The University of Texas at Austin, Austin, Texas 78712, USA*

[3]*National Laboratory of Solid State Microstructures and School of Physics, Nanjing University, Nanjing 210093, China*

[4]*School of Physics and Engineering, Zhengzhou University, Zhengzhou 450001, China*

[5]*Key Laboratory of Strongly-Coupled Quantum Matter Physics, Chinese Academy of Sciences, School of Physical Sciences, University of Science and Technology of China, Hefei, Anhui 230026, China*

[*] Present address: Department of Physics and Astronomy, Rutgers University, Piscataway, New Jersey 08854, USA

[†] Corresponding authors: Prof. Ping Cui and Prof. Zhenyu Zhang,

E-mail: cuipg@ustc.edu.cn and zhangzy@ustc.edu.cn

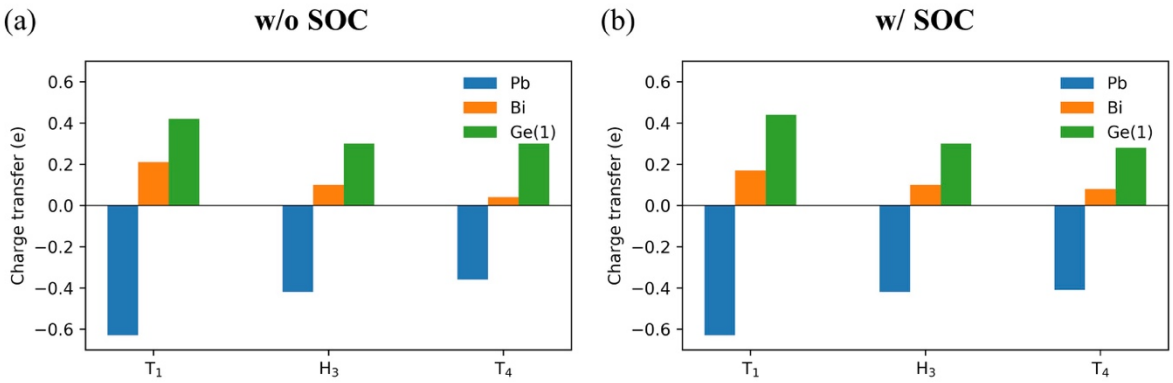

Figure S1. Calculated charge transfer from the Pb, Bi, and Ge(1) atoms in the T_1 , H_3 , and T_4 configurations (a) without SOC and (b) with SOC. The negative and positive values represent electron depletion and accumulation, respectively.

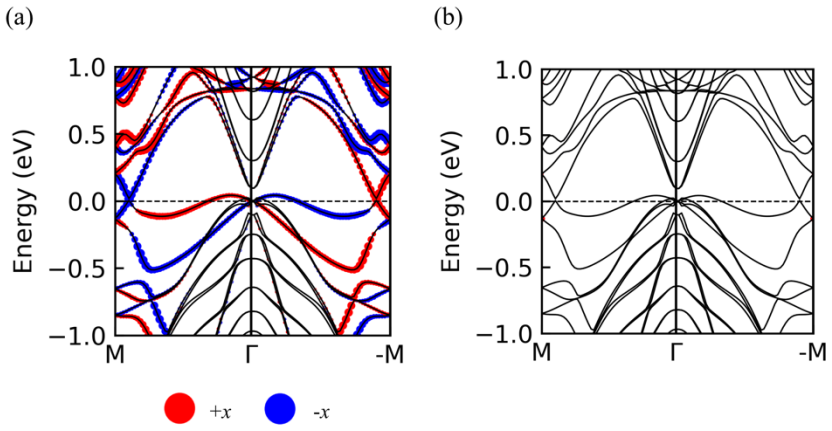

Figure S2. Band structures along the M→ Γ →-M line in the momentum space with spin component projections along the (a) *x* and (b) *y* directions of the Pb-Bi overlayer for the T_1 configuration calculated with SOC.

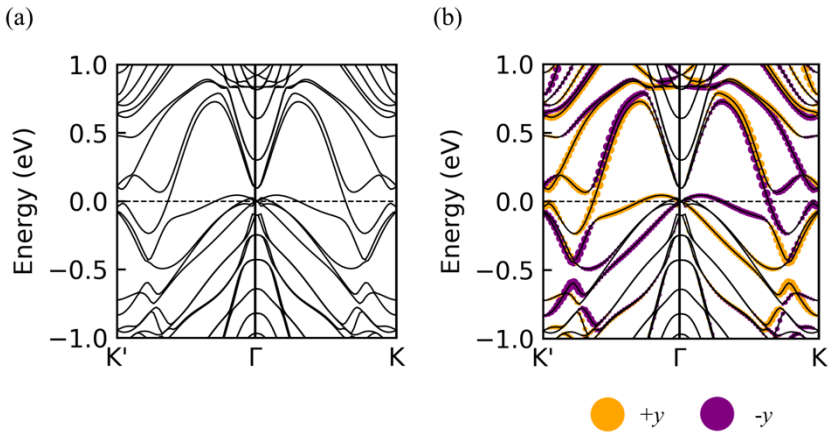

Figure S3. Band structures along the K'→ Γ →K line with spin component projections along the (a) *x* and (b) *y* directions of the Pb-Bi overlayer for the T_1 configuration calculated with SOC.

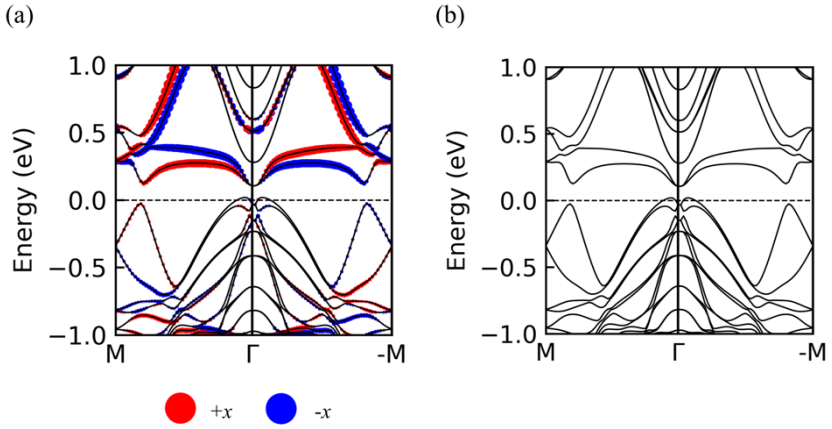

Figure S4. Band structures along the M→ Γ →-M line with spin component projections along the (a) *x* and (b) *y* directions of the Pb-Bi overlayer for the H_3 configuration calculated with SOC.

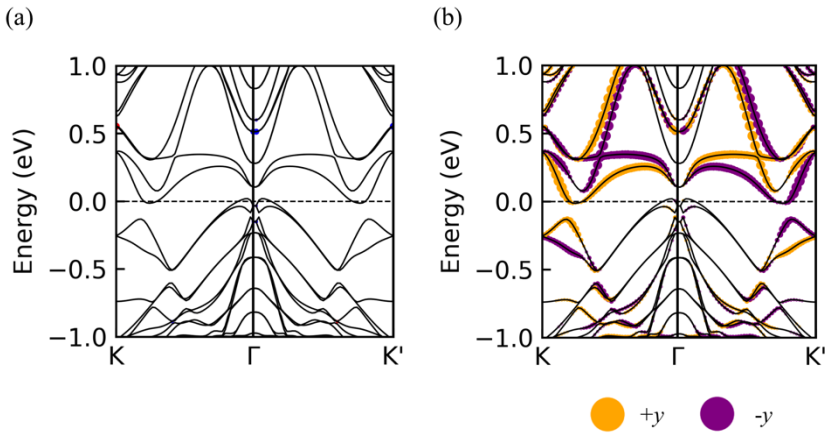

Figure S5. Band structures along the K'→ Γ →K line with spin component projections along the (a) *x* and (b) *y* directions of the Pb-Bi overlayer for the H_3 configuration calculated with SOC.

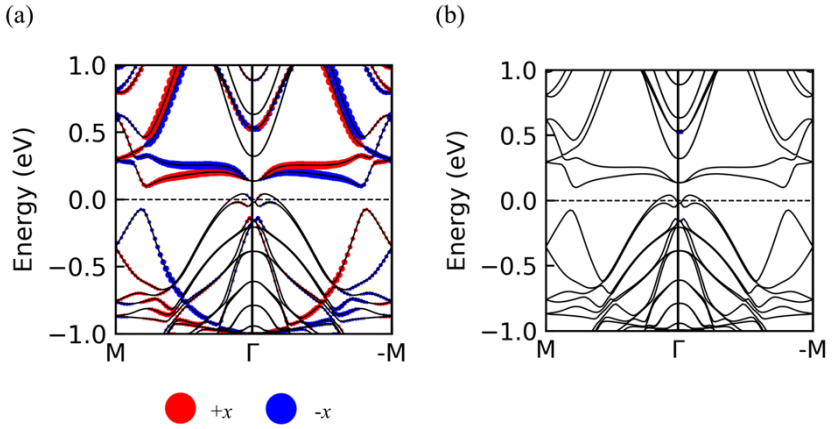

Figure S6. Band structures along the M→ Γ →-M line with spin component projections along the (a) *x* and (b) *y* directions of the Pb-Bi overlayer for the T_4 configuration calculated with SOC.

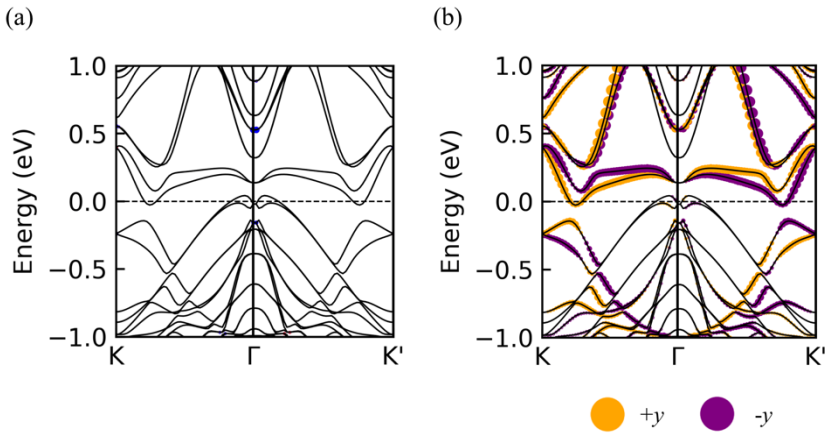

Figure S7. Band structures along the K'→ Γ →K line with spin component projections along the (a) *x* and (b) *y* directions of the Pb-Bi overlayer for the T_4 configuration calculated with SOC.

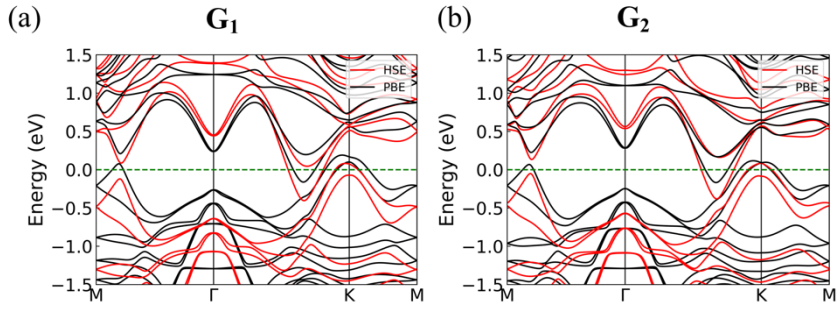

Figure S8. Band structures obtained using the PBE+SOC and HSE06+SOC schemes for the substrate-reduced (a) G_1 and (b) G_2 configurations.